Title
Modelling of rift propagation on Ronne Ice Shelf, Antarctica, and sensitivity to climate change

Journal
Geophysical Research Letters, 31(16)

ISSN
0094-8276

Authors
Larour, E
Rignot, E
Aubry, D

Publication Date
2004

DOI
10.1029/2004gl020077

Modelling of rift propagation on Ronne Ice Shelf, Antarctica, and sensitivity to climate change

E. Larour,[1] E. Rignot,[1] and D. Aubry[2]

Received 24 March 2004; revised 24 June 2004; accepted 14 July 2004; published 31 August 2004.

[1] The calving of icebergs from large Antarctic ice shelves is controlled mainly by the formation and propagation of rifts originating from the side margins of the ice shelf and local areas of grounding. Using InSAR, we observe the evolution of rifts along Hemmen Ice Rise, on Ronne Ice Shelf, Antarctica prior to the large calving event of October 1998. We couple these observations with a computer model combining the viscous flow of an ice shelf with a linear elastic fracture mechanics description of the propagation of rifts. The model reveals that the ice melange trapped in between the rifts exerts a major control on the propagation of rifts, and in turn on ice shelf stability. Melting of the ice melange from oceanic or atmospheric warming would significantly increase the propagation rate of rifts and threaten the ice-shelf stability. *INDEX TERMS:* 0933 Exploration Geophysics: Remote sensing; 1827 Hydrology: Glaciology (1863); 1863 Hydrology: Snow and ice (1827); 5104 Physical Properties of Rocks: Fracture and flow. **Citation:** Larour, E., E. Rignot, and D. Aubry (2004), Modelling of rift propagation on Ronne Ice Shelf, Antarctica, and sensitivity to climate change, *Geophys. Res. Lett.*, *31*, L16404, doi:10.1029/2004GL020077.

1. Introduction

[2] Large Antarctic ice shelves discharge ice into the oceans mainly from the calving of large tabular icebergs. These icebergs form when the ice shelf ruptures, typically along lines of pre-existing weaknesses or rifts, which are fractures that penetrate through the entire ice column thickness. Rifts originate from thickness cracks in regions of high stress, such as the ice shelf side margins, ice rises, or in areas of intense longitudinal stretching of the ice [*Vaughan*, 1993; *Weertman*, 1973; *Van der Veen*, 1998]. While a lot of work has been done understanding the propagation of cracks in sea ice [e.g., *Defranco and Dempsey*, 1991], the processes controlling the formation and propagation of rifts into an ice shelf remain poorly understood. As a result, there is no realistic calving law for an ice shelf that can easily be incorporated in a computer model of ice sheet/ice shelf flow evolution.

[3] Here, we present a model describing the evolution of rifts near Hemmen Ice Rise (HIR), on the Ronne Ice Shelf, Antarctica, prior to the large calving event of October 1998 which resulted in the formation of iceberg A38. We use interferometric synthetic-aperture radar (InSAR) images collected by the ERS-1, ERS-2 and Radarsat-1 satellites for initialization of the model and for validation of the results. The model couples the forward viscous ice flow model of *MacAyeal et al.* [1998] with the Linear Elastic Fractures Mechanics (LEFM) propagation model of *Larour et al.* [2004]. We employ a control method based on the work by *MacAyeal* [1992, 1993] and *Rommelaere and MacAyeal* [1997] to infer the distributions of the ice-shelf rheology and thickness that best fits the InSAR data. This parameter selection is then used to calculate the evolution of ice shelf rifts with time and compare the results with observations.

2. Observations and Modelling

2.1. Ice Shelf Model

[4] We previously showed that the propagation of rifts in an ice shelf is well described by LEFM [*Larour et al.*, 2004]. The propagation rate of rifts is proportional to their opening rate (or velocity differential across rift)

$$\frac{da}{dt} = \frac{a\Delta\dot{u}}{c\Delta u} \tag{1}$$

where a is the rift length, $\Delta\dot{u}$ is the velocity differential across the rift at the beginning of the rift (opposite end of rupture tip), and c is a factor that accounts for the stick-slip mechanism of propagation [*Parsons et al.*, 1989], $c = 1.78$). $\Delta\dot{u}$ is known in 1992, 1996 and 1997 from InSAR [*Larour et al.*, 2004].

[5] The ice shelf velocity field is calculated using the finite element model of ice shelf flow by *MacAyeal* [1989]. At each time increment, we evaluate $\Delta\dot{u}$ across each rift, and calculate the propagation rate using equation (1). The model parameters are the ice-shelf geometry and ice thickness. Ice thickness is initially deduced from ice-shelf elevations from *Bamber and Bindschadler* [1997] assuming ice is in hydrostatic equilibrium. The dynamic boundary conditions of the model are sea water pressure at the ice front and ice velocity at the grounding line. Grounding line ice velocity is from *Joughin and Padman* [2003] and *Larour et al.* [2004].

2.2. Control Method

[6] *Rignot and MacAyeal* [1998] discussed InSAR observations of HIR in 1992 and 1996. From these observations, they deduced that the ice melange trapped in between the rifts, composed of sea ice, ice-shelf debris, wind-blown snow and marine ice [*Khazendar and Jenkins*, 2003; *Østerhus and Orheim*, 1992], tends to deform coherently in response to ice-shelf motion. *MacAyeal et al.* [1998] demonstrated that the presence of a mechanically competent ice melange in between rifts, along with ice softening along the ice shelf grounding line and ice rises, were essential to explain the

[1]Jet Propulsion Laboratory, Pasadena, California, USA.
[2]Laboratoire de Mecanique des Sols, Structures et Materiaux, Ecole Centrale Paris, Chatenay Malabry, France.

0094-8276/04/2004GL020077

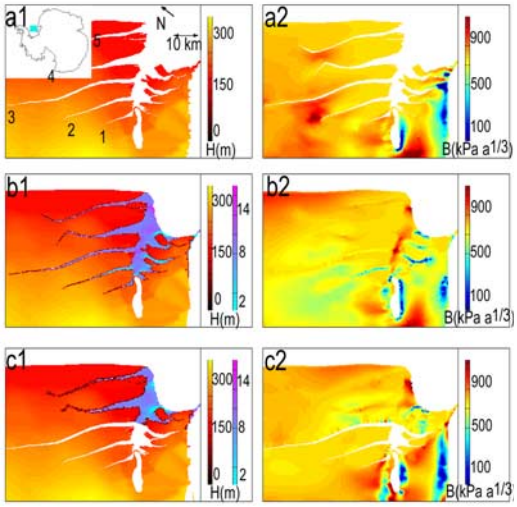

Figure 1. Panels a1, b1 and c1 show the distribution of ice thickness H (m), inferred by the control method, for respectively the water, melange and hybrid cases. Panels a2, b2 and c2 show the corresponding distribution of the flow law parameter, B (kPa $a^{1/3}$). Rifts 1 through 5 are labelled on a1.

InSAR observations. No measurement of the ice melange mechanical characteristics was available at the time. Using trial and error and a forward modelling approach, they obtained a first order model fit of the data. Here, we employ an inverse control method to achieve a better model fit, and derive the physical properties of the melange that best match the InSAR observations.

[7] The unknown model parameters are the rheology and thickness of the ice shelf and melange between rifts. Our inverse control method is based on *MacAyeal* [1992, 1993] and *Rommelaere and MacAyeal* [1997] except that we use sea water pressure as a boundary condition at the ice front instead of ice velocity. The boundary conditions on the adjoint equations are changed accordingly. Instead of using $\lambda = \mu = 0$ at the ice front, where λ and μ are the adjoint vectors, we introduce the following equations [*Woodbury*, 2003, p. 209]:

$$\int 2\eta\left(2\frac{\partial\lambda}{\partial x}+\frac{\partial\mu}{\partial y}\right)n_x+\eta\left(\frac{\partial\lambda}{\partial y}+\frac{\partial\mu}{\partial x}\right)n_y=0 \qquad (2)$$

$$\int 2\eta\left(\frac{\partial\lambda}{\partial x}+2\frac{\partial\mu}{\partial y}\right)n_y+\eta\left(\frac{\partial\lambda}{\partial y}+\frac{\partial\mu}{\partial x}\right)n_x=0 \qquad (3)$$

where η is the viscosity of the ice shelf, x and y are the ice shelf horizontal coordinates, and n_x and n_y are the components of the normal vector to the ice front. At the grounding line of the ice shelf, we keep the condition $\lambda = \mu = 0$ used by *Rommelaere and MacAyeal* [1997].

[8] Once the adjoint vectors are known across the ice shelf, we calculate the gradient of the misfit, J, between model and InSAR with respect to the unknown parameters. The first unknown is the flow law parameter, B, which appears in the definition of the viscosity, η [*MacAyeal*, 1989]. The second unknown is ice thickness, H. The calculation of the two gradients, dJ/dB and dJ/dH, as well as the steepest-descent algorithm, are similar to the ones described by *Rommelaere and MacAyeal* [1997].

[9] We model the propagation of rifts across the entire Ronne Ice Shelf. The control method is applied on the entire Ronne Ice Shelf because conditions around HIR are influenced by the evolution of the entire ice shelf, not just the surrounding ice. In particular, rifts along the western flank of the ice shelf influence ice flow around HIR. In the proximity of HIR, we use ice velocity data from *Larour et al.* [2004] and a refined mesh. To minimize computer load, we run separate control methods for B and H.

3. Results and Discussion

3.1. Control Method Results

[10] Three cases are considered: 1) rifts are filled with water; 2) rifts are filled with ice melange; and 3) young rifts are filled with water and old ones are filled with melange.

3.1.1. Water Case

[11] Ice thickness deduced from the control method is not significantly different from the initial value (Figure 1a1). The flow law parameter (Figure 1a2) exhibits significant fluctuations along the shear margins of Berkner Island and HIR. Softening of ice in these regions averages 60%, with maxima around 70–80%. This is consistent with the estimates of shear stress softening along ice stream margins by *Echelmeyer et al.* [1994], and *MacAyeal et al.* [1998].

[12] The flow model shows a large velocity differential across rift 3 (Figure 2a1). Ice located downstream of this rift is not restrained by the shear margins of Berkner Island and HIR, and therefore flows too fast in the model. Ice located

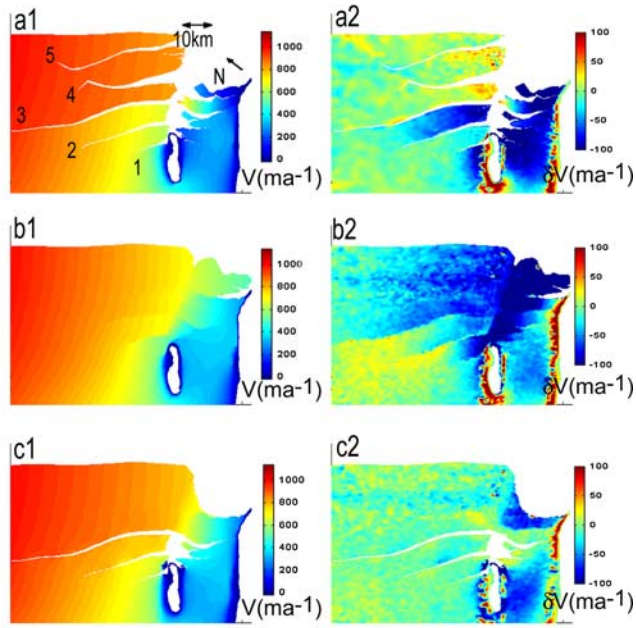

Figure 2. Panels a1, b1 and c1 show the model velocity V (m a^{-1}) inferred by the control method for, respectively, the water, melange and hybrid cases. Panels a2, b2 and c2 show the corresponding misfit between model and InSAR observations, δV (m a^{-1}).

Table 1. Propagation Rate (m a^{-1}) of Rifts[a]

Time Period	Propagation Rate 1	2	3	4	5	1σ
16/2/92 to 23/2/96	74	921	1011	0	−42	50
23/2/96 to 17/10/97	3150	371	524	−55	−55	120
17/10/97 to 2/2/98	1390	3500	4520	N/A	N/A	700

[a]Measures are between 1992 and 1998, from times series of InSAR observations. 1σ is the uncertainty in m a^{-1}.

upstream of rift 3 is conversely too slow in the model (Figure 2a2) despite softening of ice at the margins.

3.1.2. Melange Case

[13] Ice thickness between the rifts is initialized at 10 m. In Figure 1b1, the control method reveals that the ice melange in the young rifts (1–3) should be ∼4 m thin, and >10 m in the old rifts (4–5) and directly in the wake of HIR. This distribution of melange thickness is consistent with InSAR observations [*Rignot and MacAyeal*, 1998], which show that older rifts transmit ice shelf stresses more completely across rifts that younger rifts. It is also consistent with the growth of ice melange in rifts [*Østerhus and Orheim*, 1992].

[14] Similarly, the control method shows that the ice melange is softer in the most recent rifts (Figure 1b2). These new rifts are probably composed of sea ice, iceberg debris and water, so that the area-average flow law parameter of the melange is low, and stresses are not well transmitted from one side of the rift to the other.

[15] An interesting result of the control method is the inference of narrow bridges of thick ice melange between ice shelf blocks and the shear margins (Figure 1b1). This suggests the presence of ice bridges connecting ice shelf blocks. Indeed, this result is consistent with the 1997 InSAR observations which show no jump or discontinuity in interferometric phase along a large bridge between rift 4 and Berkner Island, directly in the wake of HIR, as if the ice shelf had never fractured when it crossed HIR. No line of fracture can be seen in the data. These narrow bridges appear as stiffer ice in Figure 1b2.

[16] The model (Figure 2b1) shows an acceleration of ice upstream of rift 3, and a deceleration of ice downstream. This results in a larger velocity differential across rift 2. In contrast, rift 3 is shielded by rift 2, and has a smaller velocity differential. The presence of ice melange in this case enhances cohesion of ice flow around HIR but inhibits the propagation of rift 3.

3.1.3. Hybrid Case

[17] The hybrid case was suggested by the results of the melange case. The melange is replaced by water in young rifts. It is indeed expected that when a rift opens, there is little sea ice or ice shelf debris in between. The ice melange will however quickly build up with time [*Østerhus and Orheim*, 1992]. The control method shows results similar to the melange case (Figures 1c1 and 1c2), but the misfit between the model and InSAR observations is significantly improved. Overall, the model matches the InSAR observations within ±50 m a^{-1} or 5 percent. This is the only case where the pattern of velocity differentials across rifts 1–3 is well reproduced by the model.

3.2. Propagation Results

[18] Table 1 summarizes the propagation rates of the rifts observed before the breakup. Most measurements represent annual averages, except for the last estimate which measures the propagation rate of the rift in the summer. The latter value is three times larger than the annual average, which suggests a seasonal modulation of the propagation. In the final months or weeks before the final breakup of iceberg A38, in October 1998, the propagation rate must have increased significantly (several km within days) and provoke a catastrophic rupture of the ice shelf, similar to the one observed on Pine Island Glacier [*Bindschadler and Rignot*, 2001].

[19] Figure 3 shows that active rifts originate on the margins of the ice shelf. The rifts in the middle of the ice shelf are inactive in all three simulations. This is consistent with observations of propagation rates between 1992 and 1998, which showed no significant change in length of these rifts until the final calving.

3.2.1. Water Case

[20] The model shows a rapid propagation of rift 3 (Figures 3a1 and 3a2) at rates ∼3000 m a^{-1}, or 3 times faster than in 1997, but of magnitude comparable to that observed in the months before the calving event (Table 1). Rift 2 is shielded by the propagation of rift 1, similar to the blunting effect of a field of crevasses [*Weertman*, 1973]. The rapid propagation of rift 3 is caused by the initial strong velocity differential across the rift (Figure 2a1).

3.2.2. Melange Case

[21] Figures 3b1 and 3b2 show the propagation of rifts when ice melange is present in the rifts and downstream of HIR. Rift 1 propagates at ∼1000 m a^{-1} while rifts 2 and 3 propagate at ∼200 m a^{-1} due to the blunting effect of rift 1. This blunting effect freezes the entire field of rifts. This scenario illustrates the importance of the ice melange. Its mechanical presence is sufficient to stabilize or halt the propagation of rifts. Without ice melange, rifts propagate 3 times faster, and the ice shelf is more likely to break up.

3.2.3. Hybrid Case

[22] Figures 3c1 3c2 show that rifts 2 and 3 propagate at rates ∼1000 m a^{-1}, consistent with InSAR observations

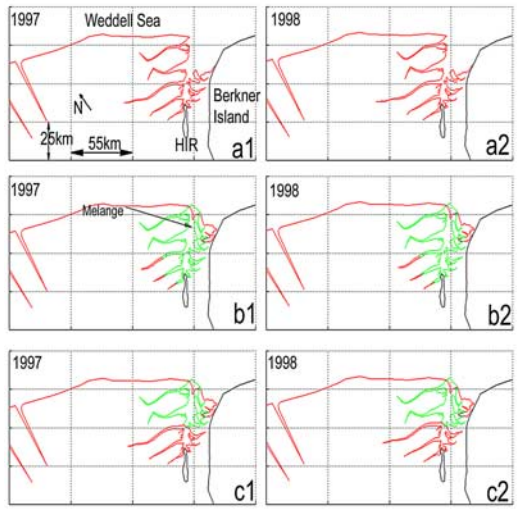

Figure 3. Distribution of rifts, respectively, in the (a1) water, (b1) melange and (c1) hybrid cases, in 1997. Panels a2, b2 and c2 show the rifts after one year of propagation. Melange boundaries are green. Ice-shelf boundaries are red.

(Table 1), yet we do not reproduce the acceleration of rifts before the final calving event. The final episode of rift propagation must have been a dynamic rupture.

4. Conclusions

[23] Our model simulations, constrained by InSAR observations using inverse control methods, show that the ice melange in between rifts exerts a stabilizing influence on the propagation of rifts into a large ice shelf and in turn on iceberg calving. The most active rifts originate on the margins of the ice shelf, where the shear stress is important. When the rifts are filled with ice melange, the propagation of rifts slows down or even halts. When the rifts are filled with water, the propagation is rapid, i.e., several times the ice velocity. In reality, our model indicates that a mixture of water and melange is required to best fit the observations. If the melange is removed, the propagation of rift 3 (which severed the entire ice shelf in October 1998) accelerates by a factor three.

[24] Thinning of the ice melange from atmospheric (top) or ocean (bottom) warming, either due to long-term changes or to seasonality, should increase the propagation rate of rifts, and precipitate the occurrence of a calving event. We would expect more rapid calving when the ice melange melts, which would explain the higher-than-annual average propagation rate in the summer (Table 1). Similarly, enhanced bottom melting from warmer ocean water intrusions under the ice shelf could thin the melange and threaten the stability of the ice shelf. The ice melange therefore provides a direct link between climate and ice shelf calving. We suggest that the recent break up of Larsen ice shelves A and B could be an example of this interaction, namely that the thinning of the ice melange by a warmer climate contributed to the sudden demise of the ice shelf along pre-existing lines of weaknesses.

[25] **Acknowledgments.** This work was performed at the Jet Propulsion Laboratory, California Institute of Technology, under a contract with the National Aeronautics and Space Administration, Cryospheric Sciences Program. We thank the European Space Agency, the VECTRA project and Alaska SAR Facility for distributing the radar data employed in this study. We thank Ian Joughin for providing his InSAR velocity observations of the Ronne ice shelf.

References

Bamber, J. L., and R. A. Bindschadler (1997), An improved elevation dataset for climate and ice-sheet modelling: Validation with satellite imagery, *Ann. Glaciol.*, *25*, 439–444.

Bindschadler, R., and E. Rignot (2001), "Crack!" in the polar night, *Eos Trans. AGU*, *82*(43), 497–498.

Defranco, S. J., and J. P. Dempsey (1991), Crack growth stability in saline ice, in *Mechanics of Creep Brittle Materials*, vol. 2, edited by A. C. F. Cocks and A. R. S. Ponter, pp. 25–36, Elsevier Sci., New York.

Echelmeyer, K. A., W. D. Harrison, C. Larsen, and J. E. Mitchell (1994), The role of the margins in the dynamics of an active ice stream, *J. Glaciol.*, *40*(136), 527–538.

Joughin, I., and L. Padman (2003), Melting and freezing beneath Filchner-Ronne Ice Shelf, Antarctica, *Geophys. Res. Lett.*, *30*(9), 1477, doi:10.1029/2003GL016941.

Khazendar, A., and A. Jenkins (2003), A model of marine ice formation within Antarctic ice shelf rifts, *J. Geophys. Res.*, *108*(C7), 3235, doi:10.1029/2002JC001673.

Larour, E., E. Rignot, and D. Aubry (2004), Processes involved in the propagation of rifts near Hemmen Ice Rise in the Ronne Ice Shelf, Antarctica, *J. Glaciol.*, in press.

MacAyeal, D. (1989), Large-scale ice flow over a viscous basal sediment: Theory and application to Ice Stream B, Antarctica, *J. Geophys. Res.*, *94*(B4), 4071–4087.

MacAyeal, D. (1992), The basal stress distribution of Ice Stream E, Antarctica, inferred by control methods, *J. Geophys. Res.*, *97*(B1), 595–603.

MacAyeal, D. (1993), A tutorial on the use of control methods in ice-sheet modeling, *J. Glaciol.*, *39*(131), 91–98.

MacAyeal, D. R., E. Rignot, and C. L. Hulbe (1998), Ice-shelf dynamics near the front of the Filchner-Ronne Ice Shelf, Antarctica, revealed by SAR interferometry: Model/interferogram comparison, *J. Glaciol.*, *44*(147), 419–428.

Østerhus, S., and O. Orheim (1992), Studies through Jutulgryta, Fimbulisen in the 1991/92 season, *FRISP Rep. 6*, pp. 103–109, Alfred-Wegener Inst. für Polar und Meeresforsch., Bremerhaven, Germany.

Parsons, B. L., J. B. Snellen, and D. B. Muggeridge (1989), The double torsion test applied to fine grained freshwater columnar ice and sea ice, in *Mechanics of Creep Brittle Materials*, vol. 1, edited by A. C. F. Cocks and A. R. S. Ponter, pp. 188–200, Elsevier Sci., New York.

Rignot, E., and D. R. MacAyeal (1998), Ice-shelf dynamics near the front of the Filchner-Ronne Ice Shelf, Antarctica, revealed by SAR interferometry, *J. Glaciol.*, *44*(147), 405–417.

Rommelaere, V., and D. R. MacAyeal (1997), Large-scale rheology of the Ross Ice Shelf, Antarctica, computed by a control method, *Ann. Glaciol.*, *24*, 43–48.

Van der Veen, C. J. (1998), Fracture mechanics approach to penetration of surface crevasses on glaciers, *Cold Reg. Sci. Technol.*, *27*, 31–47.

Vaughan, D. (1993), Relating the occurrence of crevasses to surface strain, *J. Glaciol.*, *39*(132), 255–266.

Weertman, J. (1973), Can a water-filled crevasse reach the bottom surface of a glacier?, *IAHS Publ.*, *95*, 139–145.

Woodbury, K. A. (Ed.) (2003), *Inverse Engineering Handbook*, 466 pp., CRC Press, Boca Raton, Fla.

D. Aubry, Laboratoire de Mecanique des Sols, Structures et Materiaux, Ecole Centrale Paris, Chatenay Malabry, France.

E. Larour and E. Rignot, Jet Propulsion Laboratory, 4800 Oak Grove Drive, MS 200-227, Pasadena, CA 91109-8099, USA. (eric.larour@jpl.nasa.gov)